molbank

MDPI

Short Note

trans-catena-Poly[[(bis-(μ-*N*,*N*′-bis[(pyridin-3-yl)methyl] ethanediamide))-diaqua-cadmium(II)] bis(nitrate) tetrahydrate)]

Anna Caria [1], Enrico Podda [1,2], M. Carla Aragoni [1], Riccardo Lai [1], Anna Pintus [1] and Massimiliano Arca [1,*]

[1] Dipartimento di Scienze Chimiche e Geologiche, Università degli Studi di Cagliari, S.S. 554 bivio Sestu, Monserrato, 09042 Cagliari, Italy; enrico.podda@unica.it (E.P.); aragoni@unica.it (M.C.A.); apintus@unica.it (A.P.)
[2] Centro Servizi di Ateneo per la Ricerca (CeSAR), Università degli Studi di Cagliari, S.S. 554 bivio Sestu, Monserrato, 09042 Cagliari, Italy
* Correspondence: marca@unica.it

Abstract: The reaction between cadmium nitrate tetrahydrate and *N*,*N*′-bis(pyridin-3-ylmethyl)oxalamide (**L**) in a 1:3 molar ratio in a water/acetonitrile (1:6 *v*/*v*) mixture afforded single crystals of compound **1** suitable for X-ray diffraction analysis. Compound **1** consists of the coordination polymer (CP) $[[Cd(\mathbf{L})_2(OH_2)_2](NO_3)_2{\cdot}4H_2O]_\infty$, in which Cd^{II} ions are bridged by neutral **L** antiperiplanar N-ligands in a wavy ribbon fashion developed along the *c*-axis. Two *trans*-disposed water molecules complete the pseudo-octahedral coordination geometry of the metal ion. The crystal packing of **1** revealed the interplay between π–π stacking interactions and an intricate hydrogen-bonded network involving oxalamides, nitrates, and water molecules. The donor properties of **L** and the intermolecular interactions in compound **1** are interpreted based on hybrid-DFT calculations.

Keywords: oxalamide; oxalic acid derivatives; hydrogen bonding; Cd; XRD; DFT

Citation: Caria, A.; Podda, E.; Aragoni, M.C.; Lai, R.; Pintus, A.; Arca, M. *trans-catena*-Poly[[(bis-(μ-*N*,*N*′-bis[(pyridin-3-yl)methyl] ethanediamide))-diaqua-cadmium(II)] bis(nitrate) tetrahydrate)]. *Molbank* **2024**, *2024*, M1845. https://doi.org/10.3390/M1845

Academic Editor: Nicholas Leadbeater

Received: 10 June 2024
Revised: 28 June 2024
Accepted: 30 June 2024
Published: 3 July 2024

1. Introduction

During past decades, oxamic acid derivatives, i.e., oxalic acid monoamides, have encountered a flourishing interest due to the variety of their applications, ranging from medicine [1,2] to the conservation and restoration of cultural heritage [3–6]. Oxalyl diamides (oxalamides), i.e., oxalic acid diamides, have been widely employed in synthetic organic chemistry [7,8] and coordination chemistry [9,10]. In particular, *N*,*N*′-bis(pyridin-3-ylmethyl)oxalamide (**L**) was isolated in two polymorphs [11], as a hydrate [12], and it was structurally characterized in about fifteen different cocrystals and about thirty coordination compounds, where the pyridine N-atoms were directly involved in the coordination of transition metal ions as varied as Cu^{II} [13], Zn^{II} [14], Ni^{II} [15], Ag^{I} [16], Au^{I} [17], Co^{II} [18,19], and Pd^{II} [20]. In addition, four Cd^{II} complexes bearing the **L** oxalamide ligand in combination with carboxylate and dithiophosphato ancillary ligands have been reported to date [18,21].

We report here on the synthesis and spectroscopic and structural solid-state characterization of the the coordination polymer (CP) $[Cd(\mathbf{L})_2(OH_2)_2](NO_3)_2{\cdot}4H_2O]_\infty$.

2. Results

N,*N*′-bis(pyridin-3-ylmethyl)oxalamide (**L**) was prepared in quantitative yield by refluxing pyridin-3-ylmethylamine and diethyloxalate in a 2:1 molar ratio in a water solution [6,16]. Crystals of compound **1** were grown by slow evaporation of a (1:6 *v*/*v*) acetonitrile/water mixture of **L** and $Cd(NO_3)_2{\cdot}4H_2O$ in a 1:3 molar ratio (Scheme 1; Tables S1–S4). Compound **1** was characterized by melting point determination and FTIR spectroscopy. Single crystal X-ray diffraction analysis established **1** as $[Cd(\mathbf{L})_2(OH_2)_2](NO_3)_2{\cdot}4H_2O$, crystallized in the triclinic space group $P\bar{1}$ (Figure 1).

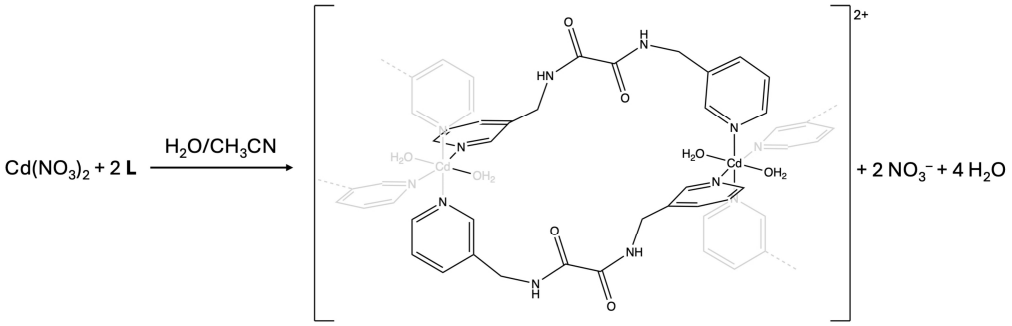

Scheme 1. Preparation scheme of $Cd(\mathbf{L})_2(OH_2)_2](NO_3)_2{\cdot}4H_2O$ (**1**) showing connectivity in the resulting CP. The sketched grey fragments are shown for completeness but are not included in the chemical balance.

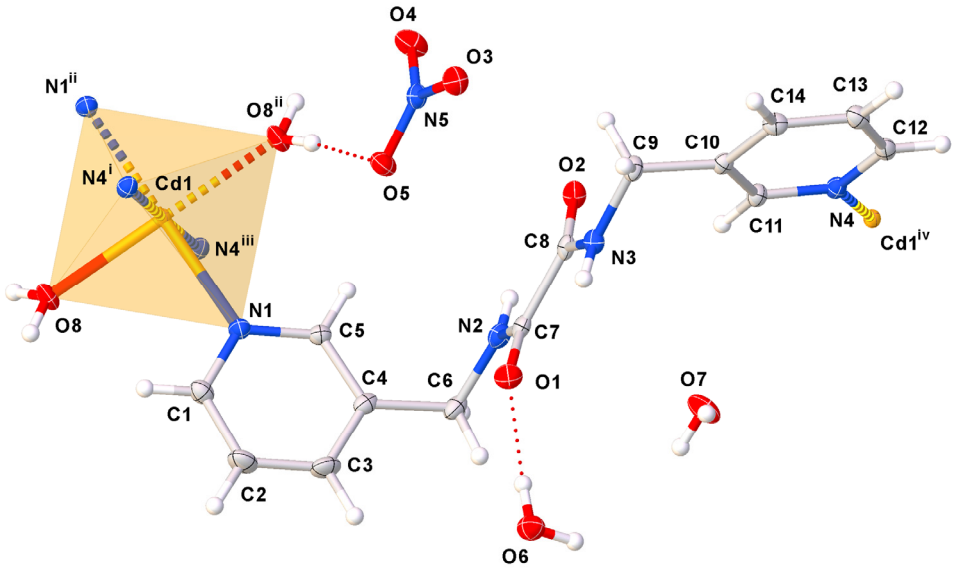

Figure 1. The X-ray crystal structure of compound **1** with a numbering scheme adopted. Displacement ellipsoids were drawn at a 50% probability level. A complete coordination sphere around the Cd^{II} ion is depicted showing symmetry-related atoms bonded through dashed bonds. Symmetry codes: $^{i} = +x, +y, 1+z$; $^{ii} = 1-x, 1-y, 2-z$; $^{iii} = 1-x, 1-y, 1-z$, $^{iv} = +x, +y, -1+z$.

The asymmetric unit of compound **1** features a half-occupied Cd^{II} ion located on an inversion centre that is coordinated by a donor molecule **L** interacting through a pyridine N1 atom [Cd1–N1 = 2.3365(10) Å], a water molecule bound to the metal ion through the O8 atom [Cd1–O8 = 2.2991(9) Å], a nitrate, and two co-crystallized water molecules. The **L** unit displays an antiperiplanar conformation of the oxalamide core with an O=C–C=O torsion angle of 174.7(1)° (Table S4), as previously found in the crystal structure determinations of different *N*,*N*′-dialkyloxalamides [22,23]. The C–C, C=O, and C–N bond lengths [1.533(1), 1.229(1)/1.233(1), and 1.325(1)/1.330(1) Å, respectively] are very close to the average values calculated for the 253 differently substituted free oxalamides deposited at the Cambridge Structural Database [CSD; average distances: C–C, 1.53(2); C–O, 1.23(1); C–N, 1.33(1) Å] [24]. Notably, all 29 compounds containing **L** that were structurally characterized show the oxalamide in the same antiperiplanar conformation.

In the crystal structure of compound **1**, each ligand unit bridges two symmetry-related Cd atoms (Cd and Cd^{iv} in Figure 1; Cd^{iv}–N4 = 2.3366(10) Å; $^{iv} = +x, +y, -1+z$), so that each Cd atom shows a pseudo-octahedral coordination achieved by four N atoms lying on the meridian coordination plane and two *trans*-disposed water molecules. This coordination results in the formation of a CP featuring a ribbon-like motif propagating along the *c*-axis with Cd nodes shared between $Cd_2\mathbf{L}_2$ links and self-complementary hydrogen bonds

between oxalamides of adjacent **L** units forming a $R_2^2(10)$ motif (interaction *a*, highlighted in light blue in Figures 2a and 3 and Table 1) [25]. In crystal packing, adjacent ribbons are connected via slipped face-to-face π–π stacking interactions [26] between pyridyl rings with distances ranging between 3.70 and 3.82 Å, as shown in Figure 2b. The charge of the cationic ribbons is balanced by NO_3^- anions that, in combination with both coordinated and co-crystallized water molecules, define an intricate hydrogen-bonded motif (interactions *b*–*h* in Figure 3 and Table 1).

A comparison between the solid-state FT-IR spectrum of compound **1** and that of the ligand **L** clearly shows the vibrational bands typical of C–H (2940–3050 cm^{-1}), N–H (3302 cm^{-1}), and C=O (1653–1655 cm^{-1}) stretching vibrations. A small but detectable shift in the C–N vibration of the pyridine ring was observed on passing from **L** to compound **1** (1525 and 1517 cm^{-1}, respectively) as a consequence of N-coordination (Figure S1). As expected, the broad band due to the O–H stretching mode of water molecules (3500 cm^{-1}) and those typical of the nitrate anion (1385 cm^{-1}) could only be envisaged in the FT-IR spectrum of compound **1**.

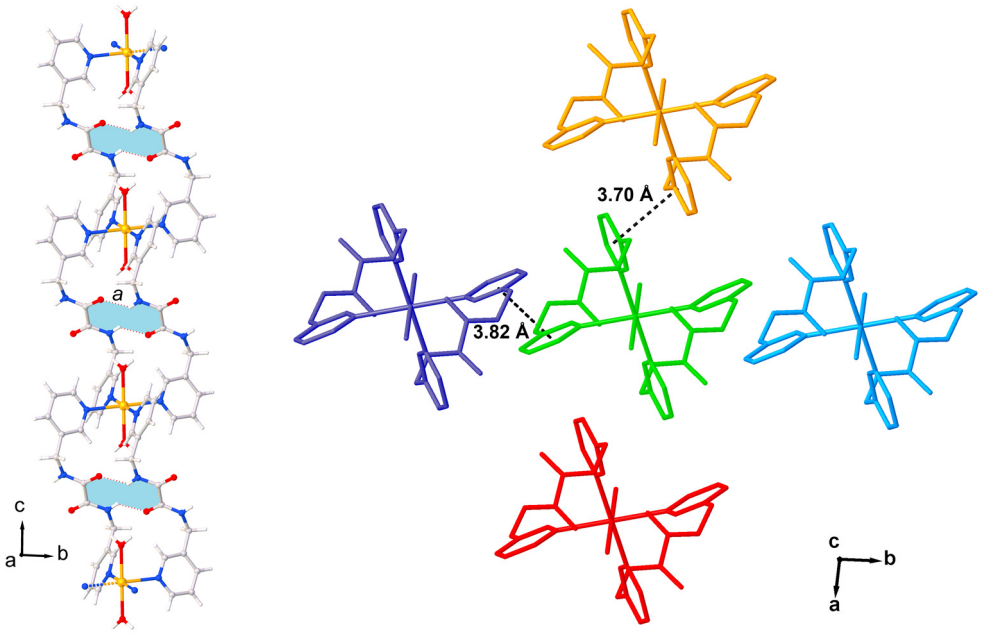

(**a**) (**b**)

Figure 2. A portion of the crystal packing of **1** showing (**a**) a single 1D-ribbon developing along the *c*-axis with the H-bonded $R_2^2(10)$ motif depicted in light blue; and (**b**) the relative orientation of adjacent 1D-ribbons along the *c*-axis. Anions and co-crystallized water molecules were omitted for clarity. Interactions are labeled according to Table 1.

Table 1. Intermolecular interactions of compound **1**.

	Interaction A–B···C	$d_{A–B}$ (Å)	$d_{B\cdots C}$ (Å)	$d_{A\cdots C}$ (Å)	$\alpha_{A–B\cdots C}$ (°)
a	N2–H2···O2^{iii}	0.83(2)	2.16(2)	2.851(2)	140.7(2)
b	O6–H6C···O1	0.78(2)	2.04(2)	2.815(2)	172.0(2)
c	O8^{ii}–H8B^{ii}···O5	0.82(2)	1.96(2)	2.775(2)	170.4(2)
d	O6–H6D···O3^{v}	0.81(2)	2.08(2)	2.876(2)	166.2(2)
e	O8–H8A···O7^{i}	0.82(2)	1.86(2)	2.674(2)	176.7(2)
f	O7–H7A···O6^{vi}	0.81(2)	1.96(2)	2.765(2)	177.2(2)
g	N3^{v}–H3^{v}···O3^{vi}	0.82(2)	2.14(2)	2.937(2)	163.6(2)
h	O7–H7B···O4^{v}	0.80(2)	2.08(2)	2.872(2)	172.7(2)

Symmetry codes: $^{i} = +x, +y, 1 + z$; $^{ii} = 1 - x, 1 - y, 2 - z$; $^{iii} = 1 - x, 1 - y, 1 - z$; $^{v} = 1 + x, +y, +z$; $^{vi} = 2 - x, 2 - y, 1 - z$.

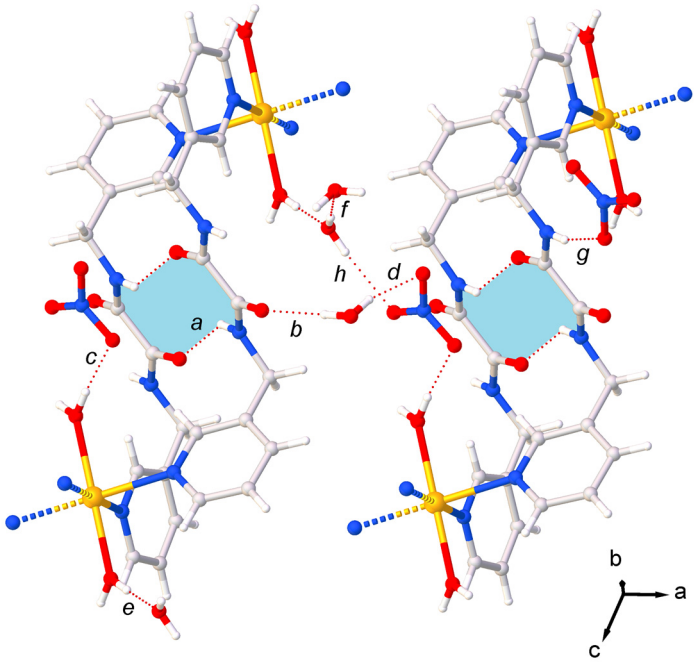

Figure 3. Hydrogen-bonding network of **1** with interactions labelled according to Table 1. The H-bonded $R_2^2(10)$ motif is depicted in light blue.

Finally, hybrid-DFT calculations showed that the lone pairs (LPs) of electrons on the pyridine nitrogen atoms of the ligand **L**, which feature remarkably negative natural charges (average charge $Q_N = -0.481$ |e|, Table S7), are available for coordination (Figure S2). Notably, the model complex cation $[Cd(\mathbf{L})_4(OH_2)_2]^{2+}$ was successfully optimized (Figure S3) and showed the same structural features as the complex unit in compound **1**. The terminal pyridine N-atoms in $[Cd(\mathbf{L})_4(OH_2)_2]^{2+}$ display natural charges ranging between −0.471 and −0.491 |e| (Table S8), demonstrating that the N-atoms on the terminal pyridine rings are available for further coordination and thus account for the formation of the CP in compound **1**.

3. Materials and Methods

3.1. General

All the reagents and solvents were used without further purification. *N*,*N*′-bis(pyridin-3-ylmethyl)oxalamide was synthesized as previously reported [16]. Fourier-transform infrared (FT-IR) spectroscopic measurements were recorded at room temperature on a Thermo-Nicolet 5700 spectrometer on KBr pellets, with a KBr beam splitter and KBr windows (4000–400 cm^{-1}; resolution 2 cm^{-1}). Melting point determinations were carried out on a FALC mod. C apparatus. DFT calculations were carried out both on **L** and the model compound $[Cd(\mathbf{L})_4(OH_2)_2]^{2+}$ at DFT level with the commercial suite of programs Gaussian 16 [27] by adopting the hybrid mPW1PW hybrid functional [28]. Double-ζ basis sets plus polarization in the def2-SVP Weigend's formulation [29,30] were adopted for all the atomic species. Vibrational frequencies were calculated at the optimized geometries. BS data were extracted from the EMSL BS Library [31]. The memory required for each calculation was evaluated by the GaussMem cross-platform (Linux, macOS, Windows) program as a function of the number of shared processors, the total number of basis set functions, and a memory threshold depending on the highest angular momentum basis function [32,33]. Molecular geometry optimization for compound **1** was performed starting from structural data. Charge distributions were evaluated at the NBO level [34–36] at the optimized geometries. GaussView v.6 [37] was used to investigate the Kohn–Sham molecular orbital composition and charge distribution. X-ray diffraction data for compound **1** were collected at 100(2) K by means of ω scans with a Bruker D8 Venture diffractometer

equipped with a PHOTON II area detector. Data reduction was carried out with SAINT v8.37 [38] and SADABS-2016/2 [39], and the structure was solved with the ShelXT [40] solution program using dual methods. The model was refined by iterative cycles of least-squares refinement on F^2 ShelXL [41] 2018/3 and by using Olex2 1.5 [42] as the graphical interface.

Crystal data for compound **1**: $C_{28}H_{40}CdN_{10}O_{16}$, ($Mr$ = 885.10 g mol^{-1}) triclinic, *P-1* (No. 2), a = 9.1489(9) Å, b = 9.2546(9) Å, c = 11.6226(12) Å, α = 91.023(4)°, β = 112.441(4)°, γ = 93.497(4) °, V = 906.96(16) Å^3, T = 100(2) K, Z = 1, μ(Mo $K\alpha$) = 0.688 mm^{-1}, 44,270 reflections measured, and 4674 unique (R_{int} = 0.0390), which were used in all calculations. The final wR_2 was 0.0425 (all data), and R_1 was 0.0167 [$F^2 \geq 2\ \sigma(F^2)$].

3.2. Synthesis of Compound **1**

To 3 mL of a CH_3CN solution of *N*,*N*′-bis(pyridin-3-ylmethyl)oxalamide (5.0×10^{-3} mol/L), a 1.0×10^{-1} mol/L solution of $Cd(NO_3)_2{\cdot}4H_2O$ in water was added (donor/Cd molar/ratio 1:3). A colourless crystalline precipitate formed in 24 h and was isolated from the mother liquor, gently washed with CH_3CN, and air-dried. A portion of the crystals was placed on a glass slide and coated with perfluoroether oil. A crystal suitable for X-ray diffraction analysis was selected and mounted on a MiTeGen loop. M.p.: 232 °C. FT-MIR (KBr pellet, 4000–400 cm^{-1}): 3508 w, 3288 m, 3057 vw, 2926 vw, 2399 vw, 2395vw, 1763 vw, 1662 s, 1606 w, 1517 m, 1452 w, 1385 vs, 1263 w, 1236 w, 1188 vw, 1128 vw, 1049 vw, 985 vw, 825 m, 750 vw, 696 m, 648 w, 511 vw, 438 vw, 407 vw cm^{-1}.

4. Conclusions

Compound **1** was synthesized by the self-assembly of *N*,*N*′-bis(pyridin-3-ylmethyl) oxalamide and cadmium nitrate and its crystal structure elucidated by single crystal X-ray diffraction analysis. The crystal structure of compound **1** consists of a CP featuring cationic 1D-ribbons whose charge is counterbalanced by nitrate anions. Each Cd node shows a pseudo-octahedral coordination achieved by four pyridine N–atoms and two *trans*-disposed water molecules. Crystal packing results from the cooperation of π–π stacking interactions and hydrogen bonds involving oxalamides, water molecules, and nitrates. Compound **1** confirms the potential of dipicolyloxalmides as flexible ligands for a variety of coordination compounds and opens new perspectives in the field of crystal engineering of CPs and metal–organic frameworks.

Supplementary Materials: Figure S1: FT-IR; Figures S2 and S3: DFT-optimized structures and Kohn–Sham molecular orbitals; Table S1: crystal data and refinement parameters; Tables S2–S4: bond lengths, bond angles, and torsion angles; Tables S5–S8: DFT-optimized geometries and natural charges.

Author Contributions: M.A. and M.C.A. Data curation: M.C.A. and E.P. Investigation: A.P., A.C., and R.L. Writing (original draft): M.A. and E.P. All authors have read and agreed to the published version of the manuscript.

Funding: The authors acknowledge the Ministero per l'Ambiente e la Sicurezza Energetica (MASE; formerly Ministero della Transizione Ecologica, MITE)—Direzione generale Economia Circolare for funding (RAEE—Edizione 2021). Fondazione di Sardegna (FdS Progetti Biennali di Ateneo, annualità 2022) is kindly acknowledged for financial support.

Data Availability Statement: Crystallographic data were deposited at the CCSD (CIF deposition number 2358751).

Acknowledgments: We acknowledge the CeSAR (Centro Servizi di Ateneo per la Ricerca) of the University of Cagliari, Italy for providing access to the SC-XRD facility.

Conflicts of Interest: The authors declare no conflicts of interest.

References

1. Qiao, T.; Xiong, Y.; Feng, Y.; Guo, W.; Zhou, Y.; Zhao, J.; Jiang, T.; Shi, C.; Han, Y. Inhibition of LDH-A by Oxamate Enhances the Efficacy of Anti-PD-1 Treatment in an NSCLC Humanized Mouse Model. *Front. Oncol.* **2021**, *11*, 1033. [CrossRef]
2. Miskimins, W.K.; Ahn, H.J.; Kim, J.Y.; Ryu, S.; Jung, Y.-S. Synergistic Anti-Cancer Effect of Phenformin and Oxamate. *PLoS ONE* **2014**, *9*, e85576. [CrossRef] [PubMed]
3. Maiore, L.; Aragoni, M.C.; Carcangiu, G.; Cocco, O.; Isaia, F.; Lippolis, V.; Meloni, P.; Murru, A.; Slawin, A.M.Z.; Tuveri, E.; et al. Oxamate Salts as Novel Agents for the Restoration of Marble and Limestone Substrates: Case Study of Ammonium *N*-Phenyloxamate. *New J. Chem.* **2016**, *40*, 2768. [CrossRef]
4. Pintus, A.; Aragoni, M.C.; Carcangiu, G.; Giacopetti, L.; Isaia, F.; Lippolis, V.; Maiore, L.; Meloni, P.; Arca, M. Density Functional Theory Modelling of Protective Agents for Carbonate Stones: A Case Study of Oxalate and Oxamate Inorganic Salts. *New J. Chem.* **2018**, *42*, 11593. [CrossRef]
5. Maiore, L.; Aragoni, M.C.; Carcangiu, G.; Cocco, O.; Isaia, F.; Lippolis, V.; Meloni, P.; Murru, A.; Tuveri, E.; Arca, M. Synthesis, Characterization and DFT-Modeling of Novel Agents for the Protection and Restoration of Historical Calcareous Stone Substrates. *J. Colloid Interface Sci.* **2015**, *448*, 320. [CrossRef] [PubMed]
6. Pintus, A.; Aragoni, M.C.; Carcangiu, G.; Caria, V.; Coles, S.J.; Dodd, E.; Giacopetti, L.; Gimeno, D.; Lippolis, V.; Meloni, P.; et al. Ammonium *N*-(pyridin-2-ylmethyl)oxamate (AmPicOxam): A Novel Precursor of Calcium Oxalate Coating for Carbonate Stone Substrates. *Molecules* **2023**, *28*, 5768. [CrossRef]
7. Dong, K.; Elangovan, S.; Sang, R.; Spannenberg, A.; Jackstell, R.; Junge, K.; Li, Y.; Beller, M. Selective Catalytic Two-Step Process for Ethylene Glycol from Carbon Monoxide. *Nat. Commun.* **2016**, *7*, 1. [CrossRef]
8. Zou, Y.Q.; Zhou, Q.Q.; Diskin-Posner, Y.; Ben-David, Y.; Milstein, D. Synthesis of Oxalamides by Acceptorless Dehydrogenative Coupling of Ethylene Glycol and Amines and the Reverse Hydrogenation Catalyzed by Ruthenium. *Chem. Sci.* **2020**, *11*, 7188. [CrossRef]
9. Chen, Z.; Jiang, Y.; Zhang, L.; Guo, Y.; Ma, D. Oxalic Diamides and Tert-Butoxide: Two Types of Ligands Enabling Practical Access to Alkyl Aryl Ethers via Cu-Catalyzed Coupling Reaction. *J. Am. Chem. Soc.* **2019**, *141*, 3541. [CrossRef]
10. Braun, M.; Frank, W.; Reiss, G.J.; Ganter, C. An N-Heterocyclic Carbene Ligand with an Oxalamide Backbone. *Organometallics* **2010**, *29*, 4418. [CrossRef]
11. Jotani, M.M.; Zukerman-Schpector, J.; Madureira, L.S.; Poplaukhin, P.; Arman, H.D.; Miller, T.; Tiekink, E.R.T. Structural, Hirshfeld surface and theoretical analysis of two conformational polymorphs of *N*,*N*′-bis(pyridin-3-ylmethyl)oxalamide. *Z. Krist. Cryst. Mater.* **2016**, *231*, 415. [CrossRef]
12. DeHaven, B.A.; Chen, A.L.; Shimizu, E.A.; Salpage, S.R.; Smith, M.D.; Shimizu, L.S. Interplay between Hydrogen and Halogen Bonding in Cocrystals of Dipyridinylmethyl Oxalamides and Tetrafluorodiiodobenzenes. *Cryst. Growth Des.* **2019**, *19*, 5776. [CrossRef]
13. Zeng, Q.; Li, M.; Wu, D.; Lei, S.; Liu, C.; Piao, L.; Yang, Y.; An, S.; Wang, C. Organic−Inorganic Hybrid Aligned by the Ligand−Ligand Hydrogen Bonds by Using Pyridyl-Substituted Oxalamides as the Building Blocks. *Cryst. Growth Des.* **2008**, *8*, 869. [CrossRef]
14. Hu, J.-H.; Hsu, H.-H.; Chen, Y.-W.; Chen, W.-H.; Liu, S.-M. Zinc(II) coordination polymers with mixed ligands: Synthesis, structures and evaluation on metal sensing. *J. Mol. Struct.* **2023**, *1289*, 135896. [CrossRef]
15. Lee, W.-T.; Liao, T.-T.; Chen, J.-D. Nickel(II) Coordination Polymers Supported by Bis-pyridyl-bis-amide and Angular Dicarboxylate Ligands: Role of Ligand Flexibility in Iodine Adsorption. *Int. J. Mol. Sci.* **2022**, *23*, 3603. [CrossRef]
16. Schauer, C.L.; Matwey, E.; Fowler, F.W.; Lauher, J. Controlled Spacing of Metal Atoms via Ligand Hydrogen Bonds. *J. Am. Chem. Soc.* **1997**, *119*, 10245. [CrossRef]
17. Wheaton, C.A.; Puddephatt, R.J. Complexes of gold(I) with a chiral diphosphine and bis(pyridine) ligands: Isomeric macrocycles and a polymer. *Polyhedron* **2016**, *120*, 88. [CrossRef]
18. Chen, W.-J.; Lee, C.-Y.; Huang, Y.-H.; Chen, J.D. Cd(II) and Co(II) coordination polymers constructed from N,N′-Bis(3-pyridylmethyl)oxalamide and 1,4-naphthalenedicarboxylic acid. *Polyhedron* **2022**, *223*, 115991. [CrossRef]
19. Liao, T.-T.; Lin, S.-Y.; Chen, J.-D. Co(II) coordination polymers supported by a benzenetetracarboxylate and bis-pyridyl-bis-amides with different flexibilities. *CrystEngComm* **2023**, *25*, 1723. [CrossRef]
20. Qin, Z.; Jennings, M.C.; Puddephatt, R.J. Self-Assembly in Palladium(II) and Platinum(II) Chemistry: The Biomimetic Ap-proach. *Inorg. Chem.* **2003**, *42*, 1956. [CrossRef] [PubMed]
21. Tan, Y.S.; Yeo, C.I.; Kwong, H.C.; Tiekink, E.R.T. Unusual {$\cdots$HNC$_2$O$\cdots$HC$_n$O}, n = 1 or 2, synthons predominate in the molecular packing of one-dimensional coordination polymers, {Cd[S$_2$P(OR)$_2$]$_2$(^{3}LH$_2$)}$_n$, for R = Me and Et, but are precluded when R = i-Pr; ^{3}LH$_2$ = *N*,*N*′-bis(3-pyridylmethyl)oxalamide. *CrystEngComm* **2022**, *24*, 2992. [CrossRef]
22. Podda, E.; Dodd, E.; Arca, M.; Aragoni, M.C.; Lippolis, V.; Coles, S.J.; Pintus, A. *N*,*N*′-Dipropyloxamide. *Molbank* **2024**, *2024*, M1753. [CrossRef]
23. Podda, E.; Dodd, E.; Arca, M.; Aragoni, M.C.; Lippolis, V.; Coles, S.J.; Pintus, A. *N*,*N*′-Dibutyloxamide. *Molbank* **2023**, *2023*, M1677. [CrossRef]
24. CSD. *ConQuest Software*, version 2024.1.0; The Cambridge Crystallographic Data Centre: Cambridge, UK, 2024.
25. Etter, M.C. Encoding and decoding hydrogen-bond patterns of organic compounds. *Acc. Chem. Res.* **1990**, *23*, 120. [CrossRef]
26. Hunter, C.A.; Sanders, J.K.M. The nature of $\pi-\pi$ interactions. *J. Am. Chem. Soc.* **1990**, *112*, 5525. [CrossRef]

27. Frisch, M.J.; Trucks, G.W.; Schlegel, H.B.; Scuseria, G.E.; Robb, M.A.; Cheeseman, J.R.; Scalmani, G.; Barone, V.; Petersson, G.A.; Nakatsuji, H.; et al. *Gaussian 16 (rev. C.01)*; Gaussian, Inc.: Wallingford, CT, USA, 2016.
28. Adamo, C.; Barone, V. Exchange functionals with improved long-range behavior and adiabatic connection methods without adjustable parameters: The mPW and mPW1PW models. *J. Chem. Phys.* **1998**, *108*, 664. [CrossRef]
29. Weigend, F.; Ahlrichs, R. Balanced basis sets of split valence, triple zeta valence and quadruple zeta valence quality for H to Rn: Design and assessment of accuracy. *Phys. Chem. Chem. Phys.* **2005**, *7*, 3297. [CrossRef]
30. Weigend, F. Accurate Coulomb-fitting basis sets for H to Rn. *Phys. Chem. Chem. Phys.* **2006**, *8*, 1057. [CrossRef] [PubMed]
31. Pritchard, B.P.; Altarawy, D.; Didier, B.; Gibson, T.D.; Windus, T.L. New Basis Set Exchange: An Open, Up-to-Date Resource for the Molecular Sciences Community. *J. Chem. Inf. Model.* **2019**, *59*, 4814. [CrossRef] [PubMed]
32. Aragoni, M.C.; Podda, E.; Chaudhari, S.; Bhasin, A.K.K.; Bhasin, K.K.; Coles, S.J.; Orton, J.B.; Isaia, F.; Lippolis, V.; Pintus, A.; et al. An experimental and theoretical insight into I_2/Br_2 oxidation of bis(pyridin-2-yl)diselane and ditellane. *Chem.—Asian. J.* **2023**, *18*, e202300836. [CrossRef] [PubMed]
33. Arca, M. GaussMem. 2024. Available online: https://massimiliano-arca.itch.io/gaussmem (accessed on 29 June 2024).
34. Reed, A.E.; Weinstock, R.B.; Weinhold, F. Natural population analysis. *J. Chem. Phys.* **1985**, *83*, 735. [CrossRef]
35. Reed, A.E.; Weinhold, F. Natural localized molecular orbitals. *J. Chem. Phys.* **1985**, *83*, 1736. [CrossRef]
36. Reed, A.E.; Curtiss, L.A.; Weinhold, F. Intermolecular interactions from a natural bond orbital, donor-acceptor viewpoint. *Chem. Rev.* **1988**, *88*, 899. [CrossRef]
37. Dennington, R.; Keith, T.A.; Millam, J.M. *GaussView*, version 6; Semichem Inc.: Shawnee Mission, KS, USA, 2016.
38. *APEX3, SAINT v8.37A*; Bruker AXS Inc.: Madison, WI, USA, 2015.
39. *SADABS-2016/2*; Bruker AXS Inc.: Madison, WI, USA, 2016.
40. Sheldrick, G.M. SHELXT—Integrated Space-Group and Crystal-Structure Determination. *Acta Cryst.* **2015**, *A71*, 3. [CrossRef]
41. Sheldrick, G.M. Crystal Structure Refinement with SHELXL. *Acta Cryst.* **2015**, *C71*, 3.
42. Dolomanov, O.V.; Bourhis, L.J.; Gildea, R.J.; Howard, J.A.K.; Puschmann, H. OLEX2: A Complete Structure Solution, Refinement and Analysis Program. *J. Appl. Crystallogr.* **2009**, *42*, 339. [CrossRef]